Constraining Earth's Core Composition from Inner Core Nucleation.

Alfred J. Wilson[1], Christopher J. Davies[1], Andrew M. Walker[2], Dario Alfè[3,4,5]

[1]School of Earth and Environment, University of Leeds, Leeds, UK, LS2 9JT; [2]Department of Earth Sciences, University of Oxford, Oxford, UK, OX1 2JD; [3]Department of Earth Sciences, University College London, London, UK, WC1E 6BT; [4]University College London, London Centre for Nanotechnology, Thomas Young Centre, London, UK, WC1H 0AH; [5]Universita‘ di Napoli “Federico II”m Dipartimento di Fisica “Ettore Pancini”, Napoli, Italy, 80126
Email: a.j.wilson1@leeds.ac.uk

This manuscript will be submitted to Proceedings of the National Academy of Sciences of the United States of America.

Constraining Earth's core composition from inner core nucleation

Alfred J. Wilson[a,1], **Christopher J. Davies**[a], **Andrew M. Walker**[b], **and Dario Alfè**[c,d,e]

This manuscript was compiled on July 31, 2024

Growth of Earth's solid inner core drives the geodynamo, generating a global magnetic field that protects the atmosphere and surface from harmful solar radiation. Yet despite its importance, the origins of the inner core remain enigmatic. Traditional models of inner core evolution ignore the physical requirement that liquids must be supercooled below their melting temperature before freezing. Recent estimates of the supercooling required to homogeneously nucleate the inner core from a variety of iron alloys are unrealistically large and incompatible with the current size and thermal structure of the inner core. Here we show, using molecular dynamics simulations, that nucleation of solids from an $Fe_{1-x}C_x$ liquid with x = 0.1-0.15 reduces the required supercooling to 250-400 K, which is consistent with present-day thermal profiles. Though our required compositions are not a complete description of core chemistry, which requires at least ternary systems, they are consistent with a number of constraints derived from seismology, mineral physics, and geochemistry. Crucially, our demonstration that specific compositions are able to account for the formation of the inner core shows that the nucleation process can provide a new and strong constraint on core composition. The estimated supercooling has implications for the thermal evolution of the core, paleomagnetic signatures of inner core formation, and the seismically observed structure of the inner core.

Inner core | Nucleation | Carbon

Significance Statement

The composition of Earth's iron-rich core influences its material properties, thermal profile, and dynamics, crucial for the geodynamo that shields the planet from harmful solar radiation. Although the core contains about 10% light elements, their exact combination is unknown. Previous studies have shown that many potential light elements are incompatible with the solid inner core's freezing. This study finds carbon is the only element tested that can explain the initial freezing and shows that the initial nucleation of the inner core offers a new constraint on the core's composition. Carbon alone cannot satisfy other constraints imposed by seismology but any viable composition of Earth's core must be compatible with all constraints, including freezing the inner core.

The solid inner core plays a crucial role in the Earth system. Inner core growth delivers thermal and chemical buoyancy to the base of outer core, which is currently the main power source driving the dynamo that generates Earth's magnetic field (1). Before the inner core formed, around $0.5-1$ Gyr ago (1–3), the core probably cooled faster and the dynamo was likely much less efficient than today (1), suggesting a signal of inner core nucleation in the paleomagnetic record (4, 5), the timing of which is still debated (6–9). The seismically observed structure of the inner core (10, 11) also preserves a unique fingerprint of Earth's evolution because it is tied to the conditions under which the solid core nucleated and grew. Yet it is currently unclear how the inner core formed (12, 13) meaning that its role in powering the dynamo over geological time, the signatures of nucleation and growth in the palaeomagnetic record, and origin of the seismically observed structure remain enigmatic.

The traditional view of inner core growth (1–3) is that the temperature (T) at the centre of the Earth declined until it reached the melting temperature (T_m) of the constituent liquid iron alloy, at which point freezing of the inner core began. From this time forward, the inner core boundary (ICB) is defined by the intersection of the outer core temperature profile and the melting temperature. However, this picture is incomplete because it ignores the physical requirement that all liquids must be supercooled by an amount $\delta T = T_m - T$ below the melting temperature before solids can nucleate without remelting (14). When evaluated for conditions near the centre of Earth's core (5000-6000 K, 360 GPa), classical nucleation theory (CNT) (14) suggests that pure liquid iron should need to be supercooled by ∼700-1000 K (12, 15, 16) in order to observe a critical nucleation event which would initiate homogeneous nucleation of the inner core within 1 Gyrs. This supercooling is incompatible with observations of inner core size (12, 13).

Author affiliations: [a]School of Earth and Environment, University of Leeds, Leeds, UK, LS2 9JT; [b]Department of Earth Sciences, University of Oxford, Oxford, UK, OX1 2JD; [c]Department of Earth Sciences, University College London, London, UK, WC1E 6BT; [d]University College London, London Centre for Nanotechnology, Thomas Young Centre, London, UK, WC1H 0AH; [e]Universita' di Napoli "Federico II"m Dipartimento di Fisica "Ettore Pancini", Napoli, Italy, 80126

Author contributions: A.J.W, C.J.D, A.M.W and D.A designed research; A.J.W performed research; A.J.W, and C.J.D analysed data; and A.J.W wrote the paper.

No competing interests are declared.

[1]E-mail: a.j.wilson@leeds.ac.uk

If the present-day ICB is defined by $T = T_m$ then the allowed undercooling, estimated by $T_m - T$ evaluated at Earth's centre, is at most 419 K based on existing data for T_m and T (13), far below the supercooling of ∼700 K required for homogeneous nucleation of pure Fe liquid according to CNT. This "inner core nucleation paradox" demonstrates that either the inner core can never have formed because the required supercooling was never achieved or that it is larger than seismically observed because the required supercooling implies most of the core is cooled below the melting point.

Attempts to resolve the inner core nucleation paradox have focused on three factors: departures from the predictions of CNT; heterogeneous nucleation due to the presence of pre-existing surfaces; homogeneous nucleation in iron alloys. Atomic scale simulations of pure Fe show that nucleating a metastable body centred cubic crystal structure can reduce the required supercooling to ∼470 K (17). BCC iron is not the thermodynamically favoured structure for the conditions of Earth's core (18) as assumed by CNT. In order to examine this condition, the Sun et al., 2022 (17) prescribe the structure of the first solids to form, however other molecular dynamic calculations of nucleation in supercooled Fe (16) do not observe the BCC structure. Instead, defect rich hexagonally close packed solids are frozen from the liquid, which also conflicts with some assertions of CNT. Yet despite these inconsistencies, CNT still adequately described the results of both studies, suggesting it is suitable for studying the inner core nucleation paradox. Other physics not included in CNT, such as pressure waves and radiogenic decay processes, are not thought to offer a plausible route to resolving the paradox (12, 15).

Heterogeneous nucleation requires identification of a pre-existing solid surface to act as a nucleation site. This solid must have low solubility and high melting temperature in order to avoid dissolution or melting and remain solid in the core, high density to be able to reach the centre of the Earth where the core is first and most supercooled, and a high wetting angle which reduces the interfacial energy associated with growing solids. Precipitates that might be present in the core include oxides (19, 20) and metallic phases (12). The former have low wetting angles with metals and low density and hence are not suitable candidates for initiating inner core nucleation. The latter are denser than the core liquid, but readily dissolve or melt in metallic iron and are therefore unlikely to reach Earth's centre (12). At present there is no material known to possess the required attributes to act as a site for heterogeneous inner core nucleation, and no geophysical scenario to explain how this material was delivered to the core to facilitate inner core formation.

Earth's core is not pure iron and contains 10 wt.% of light elements (21). Silicon, sulphur, oxygen and carbon are all candidate light elements to be present in the core due to their cosmochemical abundance and solubility in liquid Fe at high temperatures (22), while the partitioning behaviour of O and C make them ideal candidates for explaining the seismically observed density contrast at the inner core boundary (2, 23, 24). Studies of nucleation in binary Fe alloys containing these light elements have revealed that S and Si hinder nucleation (13), while O and C both increase the rate of nucleation events (13, 15). The effect is inconsequentially small for O and only low concentrations have been tested for C. The emerging picture of homogeneous nucleation in iron alloys at high pressure and temperature is that several potential binary core compositions do not resolve the inner core nucleation paradox. Therefore, identifying an alloy that resolves the paradox has the potential to place a strict constraint on the composition of the Earth's core.

To date the most promising avenue for resolving the inner core nucleation paradox has come from homogeneous nucleation in $Fe_{1-x}C_x$ alloys. Wilson et al., 2023 (13) found that a molar carbon concentration (x^C) of 0.03 reduced the required supercooling to nucleate the inner core to 612±139 K meaning that a resolution to the paradox was within 54 K when including the uncertainty of these results. Higher x^C was not tested because of limitations with the molecular dynamic model used to study the $Fe_{1-x}C_x$ system by Wilson et al., 2023 (13). In this study we develop a new potential to describe $Fe_{1-x}C_x$ systems which is capable of exploring higher x^C in liquid Fe. We use this potential to calculate the required supercooling to nucleate solids within a supercooled $Fe_{1-x}C_x$ liquid at high pressure.

Results

Liquidus temperatures are calculated using two-phase coexistence simulations for compositions between $Fe_{0.98}C_{0.02}$ and $Fe_{0.9}C_{0.1}$, shown in Fig.1. Simulations are conducted at a range of T, volume (v) conditions, spanning the pressure (P) range of the inner core. At low P and x^C, T_m is comparable to the pure Fe case of Alfè, 2002 (25), the EAM of which is used for the Fe component of the model used in this study. At high P and low x^C, T_m depression is smaller than $Fe_{1-x}O_x$ of the same x (albeit at slightly lower P). T_m is depressed by a greater amount at high x^C, ∼1300 K at $x^C = 0.1$ and 330 GPa. Interpolation of results provides melting temperatures at 360 GPa, shown in Table 1.

We use classical molecular dynamic (CMD) simulations of supercooled iron alloys to study the nucleation of solids. These simulations are independent of CNT; however, CNT provides an intuitive physical picture with which to interpret the simulation results. According to CNT, the requirement for liquids to be supercooled prior to freezing via homogeneous nucleation arises from a competition between two energetic contributions to the total free energy (ΔG) associated with forming a solid nucleus in a supercooled liquid. The first contribution is the free energy release (g^{sl}) associated with transforming supercooled liquid into a solid, which is always favourable when below the melting temperature and occurs through random fluctuations in the liquid producing "solid-like" configurations of atoms. The second contribution (γ) is associated with forming an interface between the liquid and solid and is always unfavourable. These two components are scaled by the volume and surface area of the newly formed nucleus of radius r such that

$$\Delta G(r) = \frac{4}{3}\pi r^3 g^{sl} + 4\pi r^2 \gamma. \quad [1]$$

The rate I at which a nucleus of radius r forms is defined by Boltzmann statistics:

$$I(r) = I_0 \exp\left(\frac{-\Delta G(r)}{k_B T}\right), \quad [2]$$

where k_B is Boltzmann's constant and I_0 scales the nucleation rate of the specific system. Equation (2) shows that small

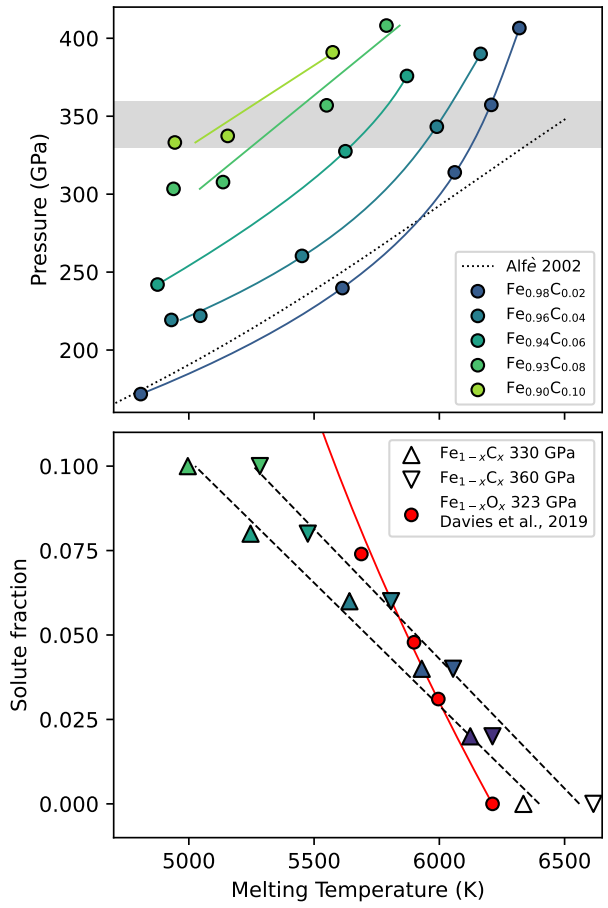

Fig. 1. Upper: Melting temperatures (points) calculated using two-phase coexistence simulations of $Fe_{1-x}C_x$ systems. Dotted line shows the melting curve of pure Fe from Alfè, 2002 (25) for reference. Solid lines are fits to data (2nd degree polynomial for x^C = 0.02, 0.04, 0.06 and linear for x^C = 0.08, 0.10). Grey shaded region shows the P range of the Earth's inner core. Lower: Interpolation of points in upper panel gives T_m(330 GPa,x^C) and T_m(360 GPa,x^C), shown as up and down pointing triangles, respectively. These conditions represent the present day inner core boundary and centre of Earth, respectively. The $Fe_{1-x}O_x$ result of Davies et al., 2019 (15) at 323 GPa is shown for comparison (red points and line).

nuclei are likely to form often (or equivalently, require less waiting time ($\tau_w \approx I^{-1}$) before they occur); however, Equation (1) shows that these nuclei will remelt rather than grow because of the large influence of surface area on the free energy at small r. Despite a low probability, continued growth is possible given a sufficiently long waiting time and large system volume to observe random fluctuations which produce a larger nucleus. Above a critical radius $r_c = -2\gamma/g^{sl}$ at the peak of ΔG the volume term in Equation (1) increases with radius faster than surface term, meaning that whilst still having an overall unfavourable free energy for forming a nucleus, continued growth is thermodynamically favoured when compared to remelting. Greater supercooling requires a smaller r_c in order to freeze a system, which in turn requires less waiting time for the critical event to spontaneously occur.

From our simulations we obtain $I(r)$ directly for sub-critical nuclei and using CNT we are then able to fit for r_c, which informs τ_w. This approach means that systems with low supercooling can be studied directly, avoiding large extrapolation necessary in prior approached (15). Critical radii r_c are estimated from $I(r)$ recorded from CMD simulations (see methods and Wilson et al., 2021 (16)) at selected temperature T and composition x^C and are shown in Fig. 2 with comparison to prior results for $x^C = 0.01$ and $x^C = 0.03$ from Wilson et al., 2023 (13). $r_c(T)$ at each x^C is then used to fit the remaining quantities h_f, h_c and γ in Eq.1. Finally, the waiting times τ_w for nucleation can be predicted for the inner core.

The interatomic potential developed here reproduces the r_c result of Wilson et al,. 2023 (13) at $x^C = 0.01$ and 5000 K within 4% (r_c = 9.16 ±1.86 Å compared to r_c = 9.52±2.31 Å(13)). At all tested values of δT, increasing x^C reduces r_c although at large δT, r_c for all compositions are within uncertainty of one another. Simulations with $x^C > 0.1$ proved unstable making tests at greater x^C impossible for the EAM developed here.

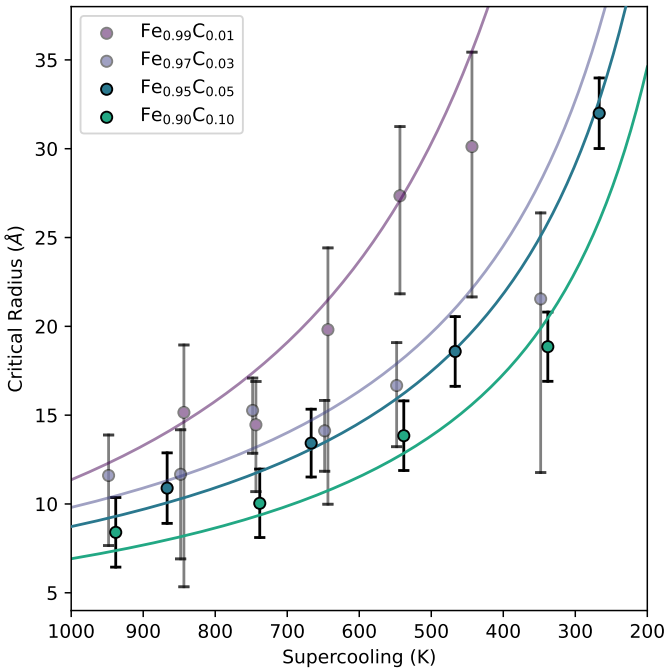

Fig. 2. Critical radii for liquid $Fe_{1-x}C_x$ alloys between x^C = 0.01 and x^C = 0.1 (x^C = 0.01 and x^C = 0.03 cases are taken from Wilson et al., 2023 (13)) all at 360 GPa. r_c is estimated from distributions of sub-critical nuclei using Eqs.14 and 15. Temperature is shown as supercooling ($\delta T = T_m - T$ where T_m is unique for each x^C, Fig.1)

Waiting times τ_w are shown in Fig. 3. Results for x^C = 0.01 and 0.03 are from Wilson et al., 2023 (13), while results for x^C = 0.05 and 0.10 are calculated using Eq.10 from the quantities shown in Table 1. The number of nucleation sites (N) and rate of nuclei growth (S) are calculated as averages from nuclei distributions and allow calculation of τ_0 using the Zeldovic factor, z (Eq.13), where $\tau_0 = \frac{z}{I_0}$. τ_0 is not found to vary with supercooling by more than one order of magnitude and so is taken as an isochemical average. Estimated waiting times are compared to the value 3.1 $\times 10^{34}$ s m^{-3}, which is a moderate waiting time the Earth's core might have sustained prior to inner core nucleation (13) (black dashed line, Fig. 3) and implies that a region with half of the present day inner core was supercooled for 1 Gyrs prior to nucleation. To produce a critical nucleation event in this waiting time, the x^C = 0.05 and x^C = 0.1 cases require $\delta T = 580^{+97}_{-71}$ K and $\delta T = 481^{+95}_{-67}$ K, respectively.

	Wilson et al., 2023		This study	
	$Fe_{0.99}C_{0.01}$	$Fe_{0.97}C_{0.03}$	$Fe_{0.95}C_{0.05}$	$Fe_{0.90}C_{0.10}$
N (m^{-3})	6.8×10^{-35}		2.3×10^{-34}	2.8×10^{-34}
S (s^{-1})	5×10^{13}		1.2×10^{12}	1.6×10^{12}
τ_0 ($s\ m^{-3}$)	2.93×10^{-23}	4.63×10^{-23}	6.48×10^{-23}	1.51×10^{-22}
h_f ($J\ m^{-3}$)	0.57×10^{10}	1.30×10^{10}	$1.35\times10^{10}\pm2\times10^{9}$	$1.55\times10^{10}\pm2.5\times10^{9}$
h_c	1×10^{-3}	1×10^{-6}	$1\times10^{-6}\pm5\times10^{-7}$	$1\times10^{-6}\pm5\times10^{-7}$
γ ($J\ m^{-2}$)	1.005	1.005	1.005 ± 0.01	1.005 ± 0.004

Table 1. Parameters defined by (N, S) and fit to (h_f, h_c, γ) distributions of sub-critical nuclei recorded in CMD simulations from Wilson et al., 2023 (13) and this study.

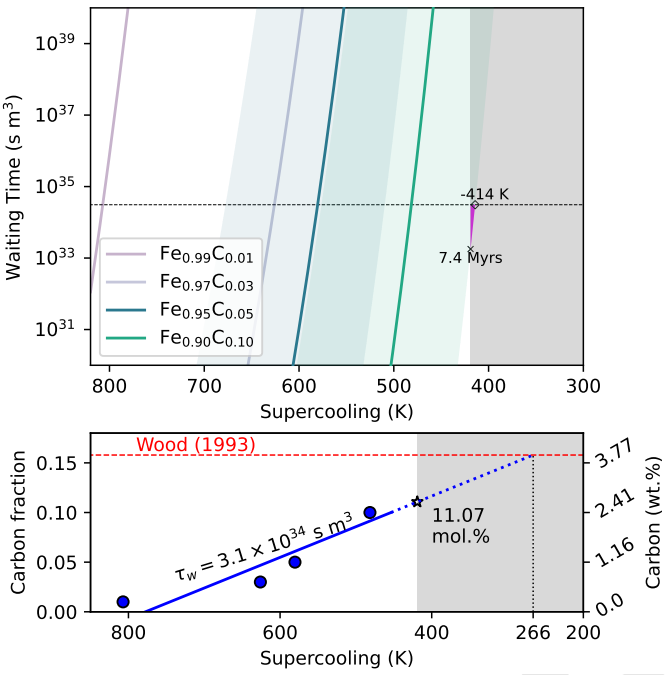

Fig. 3. Upper: Waiting time for a critical nucleation event to occur for four $Fe_{1-x}C_x$ compositions at a range of supercooling calculated using Eqs.10,12,13. Uncertainties are shown for the predictions of this study (x^C = 0.05 and x^C = 0.1) as shaded colours. Estimates from Wilson et al., 2023 (13) for x^C = 0.01 and x^C = 0.03 are also shown (without uncertainty for clarity). The dashed black line shows the maximum waiting for an inner core half its present radius supercooled for 1 Gyr and the grey shaded region represents supercooling values compatible with the present day size of the inner core (13). The pink area highlights areas of the $Fe_{0.9}C_{0.1}$ uncertainty envelop which represent a resolution to the paradox. Lower: Interpolation (solid blue line) and extrapolation (dashed blue line) of $Fe_{1-x}C_x$ results (solid lines, without exploring uncertainty) at $\tau_w = 3.1 \times 10^{34}$ s m^3 to estimate the δT needed to nucleate the inner core for values of x^C up to the maximum proposed C content of the core, $x^C = 0.156$ (red line) (26).

Discussion

Our results for a liquid carbon concentration $x^C = 0.1$ are, strictly, a resolution to the inner core nucleation paradox because the allowable supercooling of the core and the required supercooling for nucleation match within uncertainty (fig. 3). However, the value of 419 K for the allowable supercooling is a maximum obtained by considering many different published melting curves and core temperature profiles (13). It is therefore of interest to understand how the required supercooling can be further reduced below this value, which can be achieved for larger values of x^C.

The EAM developed in this study and used to define molecular dynamic simulations which characterise nucleation behaviour of $Fe_{1-x}C_x$ alloys cannot be used for x^C above 0.1. We therefore extrapolate our results at lower x^C (lower panel, Fig. 3) to predict how the supercooling requirement to spontaneously freeze the Earth's inner core might change with higher x^C. Previous studies suggest that up to 15.2 mol% (4 wt.%) C might have entered Earth's core following accretion (26). If extrapolated linearly to this concentration, given a waiting time of 3.1×10^{34} s m^3, inner core nucleation requires only 266 K of supercooling.

The melting temperature T_m at ICB conditions for a liquid carbon concentration $x^C = 0.1$ is around 5000 K (fig. 1). This value is lower than the range 5300-5900 K obtained by previous studies for the Fe-O system with O concentrations in the range 8-17 mol% (2), though it is comparable to estimates of T_m when H is a primary light element in the core (27). The corresponding core-mantle boundary (CMB) temperature, estimated by projecting an adiabat from the ICB temperature using values from the Preliminary Reference Earth Model (21) and a Grüneisen parameter in the range 1-1.5 (28) is ~3500 K, which is below estimates of the lower mantle solidus (29, 30) as required by the observed absence of pervasive melt in the lower mantle.

The true composition of the core is unknown, in part because many of the available constraints are subject to significant uncertainties (31). The true composition is likely to be more complex than the simple binary alloys we have considered (23, 32); however, it is nevertheless useful to discuss our simplified Fe-C compositions in the context of the available constraints. Geophysical constraints employ the radially-varying core density and seismic wavespeeds. C and O partition strongly into liquid iron on freezing (23, 24) and are currently the primary candidates to explain the density jump $\delta\rho$ at the inner core boundary. The C concentrations we consider are compatible with the values of the $\delta\rho$ = 0.6-1.0 gm cm^{-3} derived from seismic normal modes (33), though plausible O concentrations can also explain the $\delta\rho$ observations. Matching the core mass as well as $\delta\rho$ requires at least one other light element that partitions more evenly between inner and outer core, e.g. S or Si (23) or H (34). Ab initio calculations (27) indicate that Fe-C alloys with > 15 mol% C, compatible with resolving the nucleation paradox, can match the seismically observed CMB and ICB density as well as the CMB P-wave velocity; however, the predicted ICB P-wave velocity is higher than observed. In the inner core, the anomalously high compressional/shear wave velocity is thought to relate to the presence of small amounts of O or C (31). Geochemical constraints are derived from the inferred composition of the bulk silicate Earth (BSE) and the process of core-mantle differentiation. Depletion of the BSE compared to CI chondrites suggests that up to 15 mol% C

could be in the core (26). Recent experimental determinations of C partitioning between liquid iron alloys and silicate melts conducted in the pressure-temperature ranges 37-59 GPa and 4200-5200 K (35) and 49-71 GPa and 3600-4000 K (36) show that C becomes less siderophile as P and T increase, which when applied to a specific model of core formation indicate that C does not partition strongly into the core. However, these estimates depend strongly on mantle chemistry and the assumed core formation scenario, both of which are uncertain at present (31).

In summary, Fe-C binary alloys can satisfy some but not all constraints on the core composition. Studying nucleation is challenging even in binary alloys (13, 15) and to date no studies of ternary alloys have been attempted. Nucleation in the Fe-H system has also not been studied, though the weaker effect of H on the melting point (34) may suggest longer waiting times than we have found in the Fe-C system. Other light elements have been shown to stabilise phases of iron (37) which might nucleate more readily than those typically considered in the core (17), however, this effect has not been observed in binary systems so far (13). Ultimately, while many candidate compositions are able to reproduce available constraints from cosmochemistry (26), core differentiation (38), seismic velocities (27), and the ICB density jump (23, 24), only an Fe-C composition has so far been shown to explain the nucleation of the inner core. We therefore argue that the process of inner core nucleation can provide a novel and strong constraint on core composition. It is therefore worthwhile to reconsider previous inferences of core composition in light of this new constraint.

Inner core nucleation subject to a supercooling of 200-400 K has potentially significant implications for interpreting the structure, dynamics, and evolution of Earth's core. The predicted supercooling would delay the inner core formation age predicted by core evolution models by $O(100)$ Myrs (39, 40). In classical evolution models with high core conductivity (41) this delay would likely imply a lack of power available to the dynamo prior to inner core formation, in conflict with paleomagnetic observations (6, 7). This observation lends support to evolutionary scenarios that include long-lived dynamo power supplied by precipitation of oxides at the CMB (42–45), though the effect of C on the partitioning behaviour at the CMB has not been systematically evaluated and may influence the power provided by precipitation. Sudden rapid growth of the inner core following nucleation may leave a signature in the paleomagnetic record owing to the additional latent heat and gravitational power to the dynamo (12), though the expected influence on field intensity and variability has not yet been studied in detail. Finally, delayed inner core formation may influence texturing of the inner core, for example by trapping liquids in the solid (39), and has been correlated with the existence of the innermost inner core (40).

Materials and Methods

A. Interatomic potential. We use classical molecular dynamic (CMD) simulations of liquid $Fe_{1\text{-}x}C_x$ to characterise nucleation behaviour at a range of T and x^C. To describe the interatomic forces and system energies in our simulations, we develop an embedded atom model (EAM) which is trained on ab initio calculations. The model is fit to reproduce the positions, energy (E) and P of snapshots from ab initio molecular dynamics (AIMD) calculations run using the VASP software package (46) with the projector augmented wave method (47) and the PW91 generalised gradient approximation functional (48). Details of these calculations follow Wilson et al., 2023 (13) which shares some of the same AIMD data at low x^C used for fitting the potential. The EAM potential is validated against a separate suite of AIMB snapshots to ensure that E and P are accurately reproduced. The root mean square of fluctuations in E are determined to be 0.292 and 0.316 eV per cell at 5000 K for $Fe_{0.95}C_{0.05}$ and $Fe_{0.9}C_{0.1}$, respectively, far less than k_B/T (0.431 eV). Reproduction of liquid structure is confirmed by comparison of radial distribution functions where average positions of neighbouring atoms in CMD simulations are within 0.05 Å of AIMD simulations for all interactions and all v, T, x^C conditions.

AIMD simulations are performed by melting systems of 128 atoms with different carbon fractions (close to 20, 10 and 5 mol. %) at 10000 K for 1 ps before equilibrating at a target T (4000, 5000 and 6000 K) for 1 ps and evolving the system at the target T for 30 ps. The simulation cell volume is tuned for each composition and target T to achieve a P of 360 GPa. From the final 30 ps of simulation time, configurations are selected at every 100 fs as data on which the EAM is trained. The total energy E of a $Fe_{1\text{-}x}C_x$ system is defined by the EAM as the sum over contributions from all atomic interactions

$$E = \sum_{i=1}^{N_{Fe}} E_i^{Fe} + \sum_{i=1}^{N_C} E_i^{C} + \sum_{i=1}^{N_{FeC}} E_i^{FeC}. \quad [3]$$

Each interaction, between atoms i and j, contains repulsive Q and embedded F contributions. Q depends on the interatomic distance r_{ij} which also defines an electron density ρ_{ij} on which F depends. E for each type of interaction is given by

$$\begin{aligned} E_i^{Fe} &= Q_i^{Fe} + F^{Fe}(\rho_i^{Fe}) \\ &= \sum_{j=1,j\neq i}^{N_{Fe}} \epsilon^{Fe} \left(a^{Fe}/r_{ij}\right)^{n^{Fe}} - \epsilon^{Fe}\dot{C}^{Fe}\sqrt{\rho_i^{Fe}}, \end{aligned} \quad [4]$$

$$\begin{aligned} E_i^{C} &= Q_i^{C} + F^{C}(\rho_i^{C}) \\ &= \sum_{j=1,j\neq i}^{N_{C}} \epsilon^{C} \left(a^{C}/r_{ij}\right)^{n^{C}} - \epsilon^{C}\dot{C}^{C}\sqrt{\rho_i^{C}}, \end{aligned} \quad [5]$$

$$\begin{aligned} E_i^{FeC} &= Q_i^{FeC} \\ &= \frac{1}{2}\sum_{i=1}^{N_{Fe}} \sum_{j=1,i\neq j}^{N_{C}} \epsilon^{FeC} \left(a^{FeC}/r_{ij}\right)^{n^{FeC}}, \end{aligned} \quad [6]$$

where the respective densities are

$$\rho_i^{Fe} = \sum_{j=1,j\neq i}^{N_{Fe}} \left(a^{Fe}/r_{ij}\right)^{m^{Fe}} + \rho_i^{FeC}, \quad [7]$$

$$\rho_i^{C} = \sum_{j=1,j\neq i}^{N_{C}} \left(a^{C}/r_{ij}\right)^{m^{C}} + \rho_i^{FeC}, \quad [8]$$

and

$$\rho_i^{FeC} = \sum_{j=1,j\neq i}^{N_{C}} \left(a^{FeC}/r_{ij}\right)^{m^{FeC}}. \quad [9]$$

Here, ϵ, a, n, m and $\dot{C}$ are free parameters to be fit for each interaction and are reported in Table 2. Simulations where $x^C > 0.1$ are found to dissociate into two components, Fe rich and C rich, and are discarded from our analysis. Given the expense our calculations (∼4 million cpu hours), developing an additional EAM is not within the scope of this study.

B. Melting temperatures. The melting temperatures of $Fe_{1\text{-}x}C_x$ are calculated with coexistence simulations using the EAM potential and the LAMMPS simulation package (49). Systems of 128000 atoms are arranged into a long periodic cell where the x axis is 3 times the length of y and z axes. All atoms are initially arranged in a

	ϵ	a	n	m	$\dot{C}$
Fe	0.166200 (eV)	3.471400 Å	5.930000	4.788000	16.550000
FeC	0.384726(eV)	2.601660 Å	4.380769	4.933012	
C	0.019805(eV)	2.311113 Å	9.532860	6.967342	13.880981

Table 2. Parameters for EAM model fit to FPMD data at several C concentrations and temperatures. Fe values, from Alfè, 2002 (25), are fixed during fitting.

hexagonally close packed structure with C atoms randomly replacing Fe atoms to achieve the desired concentration. The positions of atoms in the central 50% of the simulation are initially fixed in space whilst the other half is melted at 10000 K for 5 ps. This procedure establishes the two phase system. The entire system is then evolved at a target T under the NVT ensemble for 1 ps to establish the target average kinetic energy. Finally, the system is evolved for 10 ps under the NVE ensemble, allowing the solid region of the system to grow or melt. Once the system has reached equilibrium, the T will lie on the melting curve, meaning that the time averaged T and P provide a single T_m. The random distribution of C into the initial system provides many different initial x^C for the solid and freezing and melting of the solid allows for C partitioning between the solid an the liquid. Systems with $x^C > 0.05$ in the solid see much of the solid melt before freezing a lower x^C solid. This process shows that whilst C cannot diffuse freely in the solid over the timescale of these simulations, systems tend towards chemical equilibrium through freezing and melting. Simulations which stabilise T and P have $k_D = 4\pm2$ (where $k_D = \frac{x^C_{liquid}}{x^C_{solid}}$) which is consistent with ab initio calculations (24). We estimate the uncertainties of each $T_m(v,x)$ point from the fluctuations of T and P over the final 1 ps of simulation time and discard any simulations which entirely freeze, melt, or do not achieve equilibrium. Because of the constant volume and energy conditions, T and P are unknown prior to the simulation setup. In order to define $T_m(P,x)$ we explore a range of initial T and v and interpolate our results for T_m(360 GPa,x).

C. Nucleation theory. The rate at which a nucleus of size r spontaneously forms in a supercooled liquid is given by Eq.2. When framed in terms of r_c the inverse of nucleation rate describes the average duration before a supercooled system will experience a critical nucleation event and freeze

$$\tau_w = \tau_0 \exp\left(\frac{\Delta G(r_c)}{k_B T}\right), \quad [10]$$

where

$$r_c = \frac{-2\gamma}{g^{sl}}. \quad [11]$$

The prefactor τ_0 can be described by

$$\tau_0 = \frac{z}{NS}, \quad [12]$$

where the Zeldovich factor z is related to g^{sl} through

$$z = \left(\frac{\frac{4}{3}\pi r_c^3 g^{sl}}{k_B T}\right)^{-1/2}. \quad [13]$$

and, N and S are the number of available nucleation sites and the rate of nuclei growth, respectively. To quantify N, S and $I(r)$ solid-like arrangements of atoms are identified at each timestep in the same manner as our previous studies (13, 16) following Rein et al., 1996 (50). Therefore, all quantities required to calculate τ_w are accessible via CMD calculations. Because r_c is predicted to be large for the P and T of the early Earth's supercooled liquid core (16), simulations at >5000 K and 360 GPa cannot be expected to produce a nucleus of the critical size (>30 Å). Instead, r_c is predicted by recording the rate at which smaller nuclei (which are more common) are observed in simulations, informing $I_T(r)$ where r is small. At a fixed T all quantities in Eq.1 are constant so we can write

$$-\ln\left(I_T(r)\right) \propto \Delta G_T(r) \quad [14]$$

and the distribution of nuclei observed in simulations describes the form of $\Delta G_T(r)$ but not the amplitude. Nuclei are assumed to be spherical for $r > 2$ Å, which is proven to be valid in our previous studies (13, 16) and also observed in these simulations, meaning that the form of the free energy barrier can be represented by

$$\Delta G_T(r) = 4/3\pi r^3 A + 4\pi r^2 B, \quad [15]$$

where A and B are variables at each T and r_c can be estimated via $r_c = -2B/A$, equivalent to Eq.11. If repeated for a range of T (and therefore δT) $r_c(T)$ is obtained. The free parameters γ, h_f and h_c are then found by fitting for $r_c(T)$ through

$$r_c(T) = \frac{-2\gamma}{h_f \frac{\delta T}{T_m}(1 - h_c \delta T)}, \quad [16]$$

where the h_f is the enthalpy of fusion and h_c accounts for non-linearity with temperature when defining the free energy liberated by freezing supercooled liquid

$$g^{sl} = h_f \frac{\delta T}{T}\left(1 - h_c \delta T\right). \quad [17]$$

All data used in this study is availible at the repository 10.5281/zenodo.13144422.

ACKNOWLEDGMENTS. We acknowledge a Natural Environment Research Council (NERC) grant, reference NE/T000228/1, which supports all authors on this project. AJW and CD acknowledge support from the NERC grant NE/V010867/1. AMW and CD acknowledge support from the NERC grant NE/T004835/1. DA acknowledges support from the NERC grants NE/M000990/1 and NE/R000425/1. For the purpose of Open Access, the author has applied a CC BY public copyright licence to any Author Accepted Manuscript (AAM) version arising from this submission.

1. F Nimmo, Energetics of the core in *Treatise on geophysics 2nd Edn*, ed. G Schubert. (Elsevier, Amsterdam) Vol. 8, p. 27–55 (2015).
2. C Davies, M Pozzo, D Gubbins, D Alfè, Constraints from material properties on the dynamics and evolution of Earth's core. *Nat. Geosci.* **8**, 678–685 (2015).
3. S Labrosse, Thermal evolution of the core with a high thermal conductivity. *Phys. Earth Planet. Interiors* **247**, 36–55 (2015).
4. PE Driscoll, Simulating 2 ga of geodynamo history. *Geophys. Res. Lett.* **43**, 5680–5687 (2016).
5. CJ Davies, et al., Dynamo constraints on the long-term evolution of earth's magnetic field strength. *Geophys. J. Int.* **228**, 316–336 (2022).
6. AJ Biggin, et al., Palaeomagnetic field intensity variations suggest mesoproterozoic inner-core nucleation. *Nature* **526**, 245–248 (2015).
7. RK Bono, JA Tarduno, F Nimmo, RD Cottrell, Young inner core inferred from ediacaran ultra-low geomagnetic field intensity. *Nat. Geosci.* **12**, 143–147 (2019).
8. T Zhou, et al., Early cambrian renewal of the geodynamo and the origin of inner core structure. *Nat. communications* **13**, 1–7 (2022).
9. Y Zhang, NL Swanson-Hysell, MS Avery, RR Fu, High geomagnetic field intensity recorded by anorthosite xenoliths requires a strongly powered late mesoproterozoic geodynamo. *Proc. Natl. Acad. Sci.* **119**, e2202875119 (2022).
10. A Deuss, Heterogeneity and anisotropy of earth's inner core. *Annu. Rev. Earth Planet. Sci.* **42**, 103–126 (2014).
11. H Tkalcic, *The Earth's Inner Core Revealed by Observational Seismology*. (Cambridge University Press), (2017).
12. L Huguet, JA Van Orman, SA Hauck II, MA Willard, Earth's inner core nucleation paradox. *Earth Planet. Sci. Lett.* **487**, 9–20 (2018).
13. AJ Wilson, D Alfè, AM Walker, CJ Davies, Can homogeneous nucleation resolve the inner core nucleation paradox? *Earth Planet. Sci. Lett.* **614**, 118176 (2023).
14. JW Christian, *The theory of transformations in metals and alloys*. (Newnes), (2002).
15. C Davies, M Pozzo, D Alfè, Assessing the inner core nucleation paradox with atomic-scale simulations. *Earth Planet. Sci. Lett.* **507**, 1–9 (2019).
16. AJ Wilson, AM Walker, D Alfè, CJ Davies, Probing the nucleation of iron in earth's core using molecular dynamics simulations of supercooled liquids. *Phys. Rev. B* **103**, 214113 (2021).
17. Y Sun, F Zhang, MI Mendelev, RM Wentzcovitch, KM Ho, Two-step nucleation of the earth's inner core. *Proc. Natl. Acad. Sci.* **119**, e2113059119 (2022).

18. L Stixrude, Structure of iron to 1 gbar and 40 000 k. *Phys. Rev. Lett.* **108**, 055505 (2012).
19. SM Wahl, B Militzer, High-temperature miscibility of iron and rock during terrestrial planet formation. *Earth Planet. Sci. Lett.* **410**, 25–33 (2015).
20. N Takafuji, K Hirose, M Mitome, Y Bando, Solubilities of o and si in liquid iron in equilibrium with (mg, fe) sio3 perovskite and the light elements in the core. *Geophys. Res. Lett.* **32** (2005).
21. AM Dziewonski, DL Anderson, Preliminary reference earth model. *Phys. earth planetary interiors* **25**, 297–356 (1981).
22. JP Poirier, Light elements in the earth's outer core: A critical review. *Phys. earth planetary interiors* **85**, 319–337 (1994).
23. D Alfè, M Gillan, GD Price, Composition and temperature of the Earth's core constrained by combining ab initio calculations and seismic data. *Earth Planet. Sci. Lett.* **195**, 91–98 (2002).
24. Y Li, L Vočadlo, D Alfè, J Brodholt, Carbon partitioning between the Earth's inner and outer core. *J. Geophys. Res. Solid Earth* **124**, 12812–12824 (2019).
25. D Alfè, M Gillan, G Price, Complementary approaches to the ab initio calculation of melting properties. *The J. chemical physics* **116**, 6170–6177 (2002).
26. BJ Wood, Carbon in the core. *Earth Planet. Sci. Lett.* **117**, 593–607 (1993).
27. K Umemoto, K Hirose, Chemical compositions of the outer core examined by first principles calculations. *Earth Planet. Sci. Lett.* **531**, 116009 (2020).
28. H Ichikawa, T Tsuchiya, Y Tange, The p-v-t equation of state and thermodynamic properties of liquid iron. *J. Geophys. Res. Solid Earth* **119**, 240–252 (2014).
29. D Andrault, et al., Solidus and liquidus profiles of chondritic mantle: Implication for melting of the earth across its history. *Earth planetary science letters* **304**, 251–259 (2011).
30. R Nomura, et al., Low core-mantle boundary temperature inferred from the solidus of pyrolite. *Science* **343**, 522–525 (2014).
31. K Hirose, B Wood, L Vočadlo, Light elements in the earth's core. *Nat. Rev. Earth & Environ.* **2**, 645–658 (2021).
32. K Hirose, S Labrosse, J Hernlund, Composition and state of the core. *Annu. Rev. Earth Planet. Sci.* **41**, 657–691 (2013).
33. G Masters, D Gubbins, On the resolution of density within the earth. *Phys. Earth Planet. Interiors* **140**, 159–167 (2003).
34. L Yuan, G Steinle-Neumann, Hydrogen distribution between the earth's inner and outer core. *Earth Planet. Sci. Lett.* **609**, 118084 (2023).
35. RA Fischer, E Cottrell, E Hauri, KK Lee, M Le Voyer, The carbon content of earth and its core. *Proc. Natl. Acad. Sci.* **117**, 8743–8749 (2020).
36. I Blanchard, et al., The metal–silicate partitioning of carbon during earth's accretion and its distribution in the early solar system. *Earth Planet. Sci. Lett.* **580**, 117374 (2022).
37. AS Côté, L Vočadlo, JP Brodholt, The effect of silicon impurities on the phase diagram of iron and possible implications for the earth's core structure. *J. Phys. Chem. Solids* **69**, 2177–2181 (2008).
38. J Badro, JP Brodholt, H Piet, J Siebert, FJ Ryerson, Core formation and core composition from coupled geochemical and geophysical constraints. *Proc. Natl. Acad. Sci.* **112**, 12310–12314 (2015).
39. M Lasbleis, M Kervazo, G Choblet, The fate of liquids trapped during the earth's inner core growth. *Geophys. Res. Lett.* **47**, e2019GL085654 (2020).
40. G Pang, et al., Enhanced inner core fine-scale heterogeneity towards earth's centre. *Nature* **620**, 570–575 (2023).
41. P Driscoll, C Davies, The "new core paradox:" challenges and potential solutions. *J. Geophys. Res. Solid Earth* p. e2022JB025355 (2023).
42. J Badro, et al., Magnesium partitioning between Earth's mantle and core and its potential to drive an early exsolution geodynamo. *Geophys. Res. Lett.* **45**, 13–240 (2018).
43. K Hirose, et al., Crystallization of silicon dioxide and compositional evolution of the Earth's core. *Nature* **543**, 99–102 (2017).
44. AJ Wilson, et al., Powering earth's ancient dynamo with silicon precipitation. *Geophys. Res. Lett.* **49**, e2022GL100692 (2022).
45. T Mittal, et al., Precipitation of multiple light elements to power Earth's early dynamo. *Earth Planet. Sci. Lett.* **532**, 116030 (2020).
46. G Kresse, J Furthmüller, Efficient iterative schemes for ab initio total-energy calculations using a plane-wave basis set. *Phys. review B* **54**, 11169 (1996).
47. G Kresse, D Joubert, From ultrasoft pseudopotentials to the projector augmented-wave method. *Phys. review b* **59**, 1758 (1999).
48. JP Perdew, et al., Atoms, molecules, solids, and surfaces: Applications of the generalized gradient approximation for exchange and correlation. *Phys. review B* **46**, 6671 (1992).
49. S Plimpton, Fast parallel algorithms for short-range molecular dynamics. *J. computational physics* **117**, 1–19 (1995).
50. P Rein ten Wolde, MJ Ruiz-Montero, D Frenkel, Numerical calculation of the rate of crystal nucleation in a lennard-jones system at moderate undercooling. *The J. chemical physics* **104**, 9932–9947 (1996).